

Article

Tuning the Shape of Spray-Dried Pullulan Particles Through Feed Rheological Behavior

Francesca Selmin ^{1,*}, Francesco Cilurzo ¹ and Francesco Briatico Vangosa ^{2,*}

¹ Department Pharmaceutical Sciences, Università degli Studi di Milano, Via G. Colombo, 71, 20133 Milan, Italy; francesco.cilurzo@unimi.it

² Dipartimento di Chimica, Materiali e Ingegneria Chimica “Giulio Natta”, Politecnico di Milano, Piazza Leonardo da Vinci, 20133 Milan, Italy

* Correspondence: francesca.selmin@unimi.it (F.S.); francesco.briatico@polimi.it (F.B.V.)

Abstract: Pullulan is a natural polysaccharide used in many health products, including dry powders for oral and pulmonary administration. In these cases, the control of the shape and dimensions of particles is crucial for obtaining the desired functionality. Different from other polysaccharides, pullulan cannot be easily shaped without chemical modifications or adjuvants' addition. This work aims to systematically investigate the impact of the solvent composition and polymer concentration on the possibility of tuning the pullulan particle shape by spray drying. The results revealed that the microparticle-to-fiber transition can be induced using a hydro-alcoholic solution since ethanol increased the relaxation time and reduced the evaporation rate. Furthermore, a high Péclet number during drying favors the formation of wrinkled surfaces at all feed compositions. Overall, these data evidenced the possibility of tuning the spray-dried product morphology without any processing aids, paving the way for new applications of pullulan, especially in the pharmaceutical field.

Keywords: droplet drying; diffusion; fibers; Péclet number; process–product–performance



Academic Editor: Ioannis S. Chronakis

Received: 28 September 2024

Revised: 15 December 2024

Accepted: 10 January 2025

Published: 16 January 2025

Citation: Selmin, F.; Cilurzo, F.; Briatico Vangosa, F. Tuning the Shape of Spray-Dried Pullulan Particles Through Feed Rheological Behavior. *Polysaccharides* **2025**, *6*, 7.

<https://doi.org/10.3390/polysaccharides6010007>

Copyright: © 2025 by the authors. Licensee MDPI, Basel, Switzerland. This article is an open access article distributed under the terms and conditions of the Creative Commons Attribution (CC BY) license (<https://creativecommons.org/licenses/by/4.0/>).

1. Introduction

Pullulan (PUL) is a linear, unbranched natural polysaccharide produced by the fungus *Aureobasidium pullulans*, which has attracted considerable interest in many fields. It consists predominantly of maltotriose-repeating units connected by α -(1→6) glycosidic bonds. The characteristic dimeric segments of pullulan are [\rightarrow x)- α -D-glucopyranosyl-(1→4)- α -D-glucopyranosyl-(1→)] and [\rightarrow 4)- α -D-glucopyranosyl-(1→6)- α -D-glucopyranosyl-(1→)], where x may be either 4 or 6 for the (1→4) linked segment [1]. The coexistence of both α -(1→4) and α -(1→6) in a single compound is believed to be responsible for the PUL structural flexibility and solubility, resulting in distinct film- and fiber-forming characteristics. Although expensive, PUL products are edible and biodegradable, and underivatized PUL readily dissolves in water, giving solutions with viscosity independent of heat and pH change [2]. Owing to these features, PUL has been explored as a film-forming material to develop products with different functions in food packaging, tissue engineering, and drug delivery [3]. Regarding the pharmaceutical application, the film-forming properties are used to form capsules, coatings [4], orodispersible films [5,6], and microneedles [7].

In addition to its application as film-forming material, PUL was also proposed as an excipient to engineer powders. As a matter of fact, to design dosage forms intended for pulmonary administration, PUL was exploited not only to coat existing microparticles [8], but also to tune the roughness of the powder and, therefore, to ameliorate the aerodynamic diameter [9]. Indeed, the addition of PUL to trehalose spray-dried powder produced

dimpled particles, and the number and depth of dimples appeared to be dependent on PUL concentration [10]. PUL also deeply influenced the morphology of powders when used to stabilize the structure of proniosomes. Different from maltodextrins that allowed for the preparation of spherical particles, PUL led to the formation of smooth flakes [11]. Finally, PUL was mixed with an enteric polymer to prepare microparticles intended for oral administration [12].

Despite these applications, there is little information on its behavior during the drying process and the effect of the feed composition on particle morphology. Indeed, the interplay between feedstock properties (i.e., solute diffusion coefficient and solvent latent heat) and drying conditions (i.e., temperature and flow rate of drying gas) dictates the particle's dimension and morphology. Particles may be spherical, hollow, or doughnut shaped [13,14], but filaments can be also obtained [15]. In the case of PUL, the only available data are the dimensionless Péclet numbers, representing the ratio of evaporative surface recession to mass diffusivity, which, in the case of the aqueous solution, resulted in the order of 10 [9].

Herein, we investigated the impact of PUL solution composition on the formation of particles during the spray drying process. In the first part of this study, we focused on the effect of rheological behavior and evaporation properties of PUL aqueous or hydro-alcoholic solutions. Then, the morphology and dimensions of spray-dried particles were investigated in an attempt to correlate their shape to rheological properties, solvent evaporation, and diffusion rates.

We hypothesized that the data on shear and elongational viscosity of the solution can allow us to optimize the feed composition and, therefore, PUL particles with different morphology can be spray dried.

2. Materials and Methods

2.1. Materials

Two batches of PUL at the same nominal intrinsic viscosity (PUL, by Hayashibara, Okayama, J) but coming from two different production lots, referred to as Batch 1 and Batch 2 in the present work, were used to prepare a solution in (a) MilliQ[®] water or (b) water and absolute anhydrous ethanol. The composition is reported in Table 1.

Table 1. Composition of PUL solutions. PUL concentration is expressed in terms of % PUL mass/solution mass. The hydro-alcoholic solutions were prepared by dilution of the relevant aqueous solutions. For aqueous solutions, $c^* \approx 0.593$ and $c_e \approx 5.93$; for hydro-alcoholic solutions, $c^* \approx 0.615$ and $c_e \approx 6.15$.

Feed ID	PUL	Water	Ethanol
1	15.00	85.00	-
2	12.50	87.50	-
3	10.00	90.00	-
4	7.50	92.50	-
5	7.00	93.00	-
6	5.50	94.50	-
7	5.00	95.00	-
8	1.50	98.50	-
9	0.50	99.50	-
10	12.86	75.00	12.14
11	10.71	77.13	12.76
12	8.57	78.40	13.03
13	6.43	80.19	13.38
14	6.00	80.58	13.42
15	4.71	81.68	13.61
16	4.29	82.04	13.67

To promote a complete dissolution, the solution was smoothly stirred with a roll mixer. When required, ethanol was added to the polymer aqueous solution in a 6 g solution/1 g ethanol proportion. This proportion avoided the PUL precipitation, which occurred at higher ethanol contents.

These values should be compared to the critical concentration for coil overlap, c^* , and the critical entanglement concentration, c_e . To estimate these quantities, it was assumed that [16]:

$$c_e/c^* \sim 10 \quad (1)$$

and that c^* is related to the intrinsic viscosity $[\eta]$ by [17]:

$$[\eta] = 0.77 c^{*} \quad (2)$$

The intrinsic viscosity was determined by applying the Mark–Houwink–Sakurada equation with the relevant parameters [18] as follows:

$$[\eta] = 1.956 \times 10^{-4} M_w^{0.667} \quad (3)$$

Taking M_w as molecular weight, the average value of about 530 kDa determined from dynamic light scattering (DLS) measurements (Zetasizer S, Marvern Instrument, Great Malvern, UK) and confirmed by size exclusion chromatography, c^* , and c_e resulted in 0.593 g/cm³ and 5.93 g/cm³, respectively. As the density of the PUL aqueous solutions, measured with a glass pycnometer, was almost constant at a value slightly higher than 1 g/cm³ with a very limited increase for increasing concentration, c^* and c_e resulted in 0.593% (PUL mass/solution mass) and 5.93% (PUL mass/solution mass), respectively.

As for the hydro-alcoholic solution, it is assumed that the coefficients of the Mark–Houwink–Sakurada equation and, consequently, the critical concentration for coil overlap c^* and the entanglement concentration c_e values are the same as the aqueous solution. The density of PUL hydro-alcoholic solutions was estimated as a first approximation by adopting the rule of the mixture equal to 0.963 g/cm³ c^* and c_e , resulting in 0.615% (PUL mass/solution mass) and 6.15% (PUL mass/solution mass), respectively. Therefore, the range of concentrations spanned between the concentrated and the entangled regimes.

2.2. Rheological Characterization

The solution flow behavior was investigated both in shear and in extension.

Shear rheometry was carried out through steady-state shear tests with a Modular Compact Rheometer MCR 502 (Anton Paar GmbH, Graz, Austria). A plate–plate geometry was adopted, with 50 mm diameter plates. The temperature was set at 25 °C. For the hydro-alcoholic solution, a solvent trap was used to limit ethanol evaporation. The testing protocol consisted of a series of shear rate steps, logarithmically spaced between 0.01 and 100 s^{−1}. To check any change in rheological behavior during the test, shear rates were applied from the lowest to the highest and then in the opposite direction. The viscosity curves were superimposable, and no hysteresis was observed, confirming that no structural changes occurred during the test. Tests were repeated in triplicate.

Capillary Breakup Rheometry (CaBER) was exploited to investigate the PUL solutions' extensional behavior. In this technique, a stepwise uniaxial extensional flow is imposed on a fluid filament, and all properties are estimated from the decay of its diameter in time. The liquid is placed between two parallel plates positioned at a certain distance (initial gap), and they are pulled apart quickly to the final gap distance in order to create a thin liquid filament; after the initial plate motion, no further external deformation is imposed on the liquid. Due to the generated curvature, surface tension acts as a pinching force that

causes the evolution of the liquid into a filament that reaches the rupture (Figure 1). The filament radius evolution, measured on the filament symmetry plane, R_{mid} , depends on the fluid surface tension, σ (the driving force for rupture), and viscosity or viscoelasticity of the solution (providing the force to resist the thinning) [19,20].

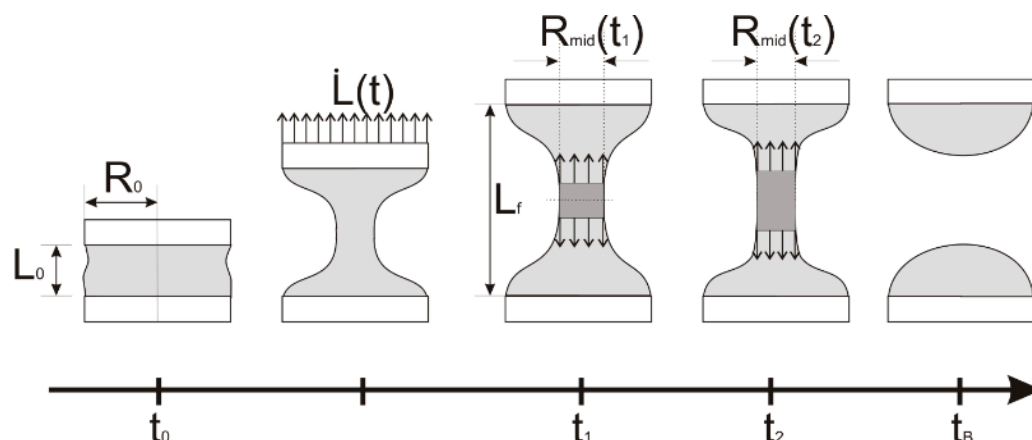


Figure 1. Schematic representation of a CaBER experiment. The liquid sample is placed between two parallel plates positioned at a certain distance (initial gap, L_0). The plates are then pulled apart quickly to the final gap distance, L_f . Due to the generated curvature, surface tension acts as a pinching force that causes the evolution of the liquid into a filament that thins out to rupture at t_B .

In case the resistance to thinning is due to the elastic response of a viscoelastic fluid, Equation (4) holds:

$$R_{mid}(t)/R_{mid}(t_1) = (1/2 (G \times R_{mid}(t_1))/\sigma)^{1/3} \exp(-t/(3\lambda_c)) \quad (4)$$

where $R_{mid}(t_1)$ is the filament radius at the end of the step stretch, G is the material shear modulus, σ is the surface tension, and λ_c is the viscoelastic material's longest relaxation time.

The measurements were performed at 25 °C using a HAAKE CaBER1 (Thermo Fisher Scientific, Karlsruhe, Germany) capillary breakup rheometer equipped with 6 mm plates. The plate distance before the step stretch was 3 mm, and the applied nominal Hencky strain, $\epsilon_H = \ln(L_f/L_0)$, was 1. R_{mid} was measured by means of the CaBER1 apparatus laser micrometer. Also, the whole filament shape was monitored to investigate the occurrence of unexpected instabilities, such as bead formation. To this end, a high-speed megapixel CMOS camera Mikrotron MC1310 (Mikrotron GmbH, Unterschleissheim, Germany) with a Computar MC TV lens, characterized by a focal length of 50 mm, was adopted. Images were acquired at a 500 fps rate with a 1000 × 1000-pixel resolution. A series of snapshots of the breakup process for a 10% aqueous solution is reported in SI.

As for the least viscous solutions, the breakup time was less than that required for the plate motion, and extensional rheometry was only carried out on the PUL solution up to 5%.

2.3. Thermogravimetric Characterization

A Thermogravimetric Analyzer TGA Q500 (TA Instruments, New Castle, DE, USA) was used to determine the solvent evaporation rate during the spray drying process and to estimate the mass transfer coefficient of the solutions. In order to reproduce as close as possible the condition undergone during spray drying, the fastest possible ramp from 25 °C to 140 °C was imposed on the sample, followed by a 40 min isothermal test at 140 °C, which is the temperature set in spray drying experiments. The testing gas was air.

The solvent evaporation from a PUL solution is governed by internal diffusion and by interfacial mass transport between the solute and the liquid phase. If the diffusion of the solvent is fast, the process is mass transfer limited, and the solvent concentration $c_s(t)$ can be estimated by Equation (5) as follows:

$$\frac{dc_s}{dt} = -h_m \frac{A}{V} c_s - \frac{c_s}{V} \frac{dV}{dt} \quad (5)$$

where A and V are the sample surface area and volume, respectively, and h_m is the mass transfer coefficient of the solvent at the solute surface [20].

As the volume cannot be assumed to be constant during the process, and it varies at a rate comparable to solvent release, the mass transfer coefficient h_m can be determined according to Equations (6)–(8) as follows:

$$h_m(t)|_{V=V(t)} = \left(\frac{dc_s(t)}{dt} + \frac{c_s(t)}{V} \frac{dV}{dt} \right) \left(\frac{V}{Ac_s(t)} \right) \quad (6)$$

$$c_s(t) = \frac{m(t) - m_{\text{solute}}}{m(t)} \quad (7)$$

$$V(t) = \frac{m(t)}{\left(\frac{6}{7} \rho_{\text{H}_2\text{O}+\text{Pul}} + \frac{1}{7} \rho_{\text{EtOH}} \right)} \quad (8)$$

where $m(t)$ is mass loss determined in TGA, m_{solute} is the mass of solute present in the sample, and $\rho_{\text{H}_2\text{O}+\text{Pul}}$ and ρ_{EtOH} are the densities of the PUL aqueous solution and ethanol, respectively. Out of the values of h_m , a Péclet (Pe) number can be defined as in Equation (9):

$$Pe = \frac{h_m L_{\text{char}}}{D} \quad (9)$$

where L_{char} is the characteristic length and D is the solute diffusion coefficient.

2.4. Spray Drying

Spray drying was carried out using a ForMate Spray Dryer 4M8 (ProCepT Processing Concept, Zelzate, Belgium) operating with a laminar and concurrent flow. The feed solution and hot gas have the same direction, and there is no turbulence in the chamber. The contact time of the hot air with the spray droplets, during which drying is achieved, is very short. A long chamber configuration, characterized by a high height (775 mm) to diameter (180 mm) ratio, was chosen to increase the particle residence time and to ensure complete drying.

The solution was sprayed through a 1 mm nozzle at a 2 bar nozzle pressure. The air and feed solution flow rates were 0.3 m³/min and 3 mL/min, respectively. The air inlet temperature was 140 °C. The air outlet temperature, as measured by a probe at the end of the drying chamber, was around 47–50 °C. The drying chamber and cyclone pressures were 3 mbar and 71 mbar, respectively.

2.5. Scanning Electron Microscopy and Image Analysis

Spray-dried samples were analyzed with Scanning Electron Microscopy with Energy-Dispersive Spectroscopy (SEM-EDS) on an Environmental SEM Zeiss EVO 50 EP equipped with an Oxford INCA 200-Pentafet LZ4 spectrometer (Zeiss, Oberkochen, Germany). The samples on a metallic stub were coated with 40–60 nm of gold and observed in high-vacuum conditions.

The SE micrographs were analyzed using ImageJ software V1.53r to measure the diameter distribution of the particles, which could be described as spherical. For each

sample, about 150 particles were measured. A magnification of $500\times$ was selected to be able to distinguish particles with diameters lower than $10\ \mu\text{m}$.

3. Results

3.1. Solution Rheology

As reported in the SI (Figure S1), all the solutions considered displayed a Newtonian behavior up to $100\ \text{s}^{-1}$, the maximum shear rate adopted in this work. The viscosity of both aqueous and hydro-alcoholic solutions increased as the concentration increased (Figure 2), and the addition of ethanol to the solution had no other effect than diluting the PUL concentration. Furthermore, no differences can be detected in the shear response for solutions prepared with both batches of PUL. Data displayed a bi-linear behavior in the log–log scale with an intercept at a concentration of $3.4\%w/w$, corresponding to the critical concentration for entanglements, which is in agreement with the estimates discussed in the Materials and Methods section. The slopes of 0.66 and about 3.67, for the low- and high-concentration batches, agreed with those expected for semi-dilute and concentrated regimes.

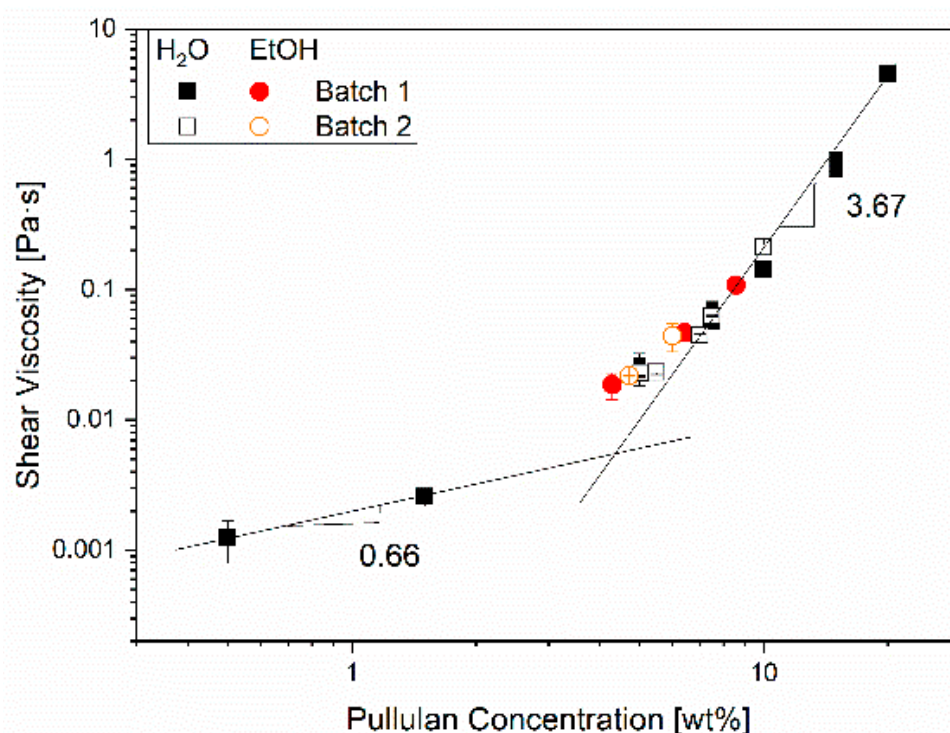
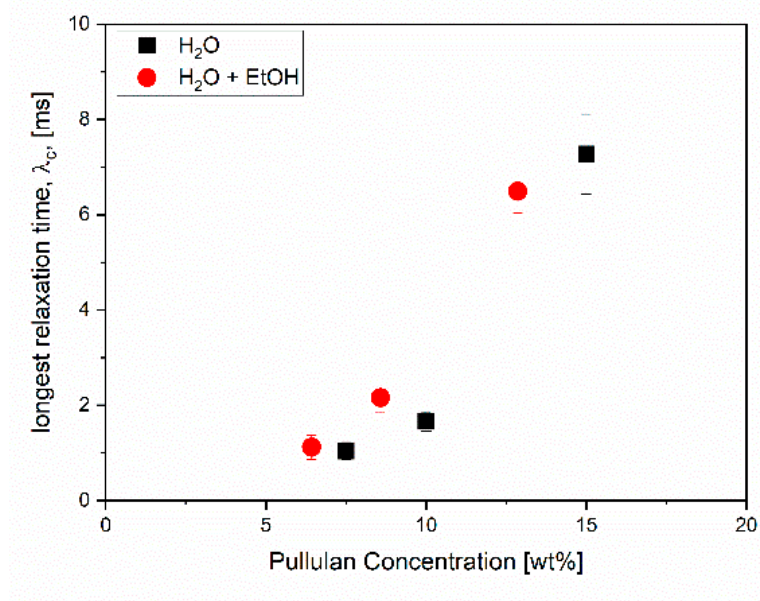
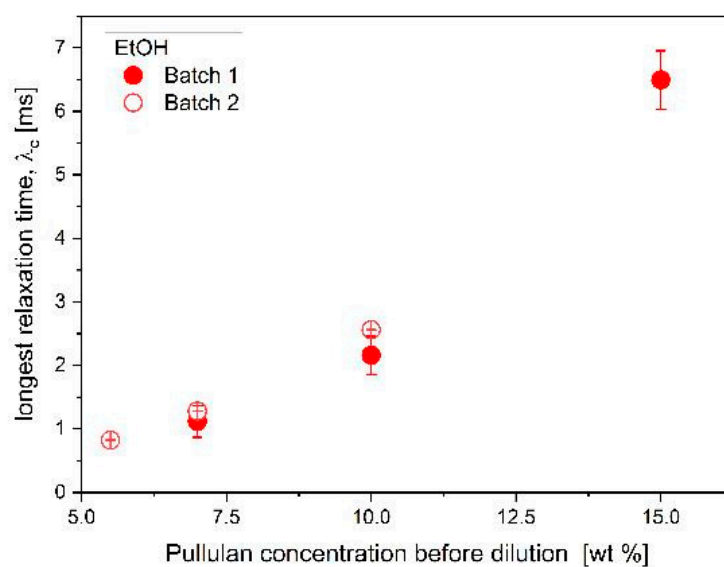


Figure 2. Effect of the concentration on the viscosity of PUL aqueous and hydro-alcoholic solutions. Filled points refer to solutions prepared from Batch 1; empty points refer to solutions from Batch 2.

Even if the shear characterization did not highlight a non-linear, viscoelastic effect, the extensional characterization revealed viscoelastic behavior, indicating that the solutions are Boger fluids [21]. Elasticity dominated the diameter evolution just before the breakup event, as evident in Figure S2, and the corresponding portion of the diameter–time curve (Figure S3) was fitted according to Equation (4). In the case of Batch 1 solutions, the longest relaxation times, λ_c , are plotted as a function of effective concentration in Figure 3a. With respect to the relaxation phenomenon, the effect of adding ethanol to the solution is not limited to a dilution effect; hydro-alcoholic solutions display slower relaxation with respect to aqueous solution with the same concentration.



(a)



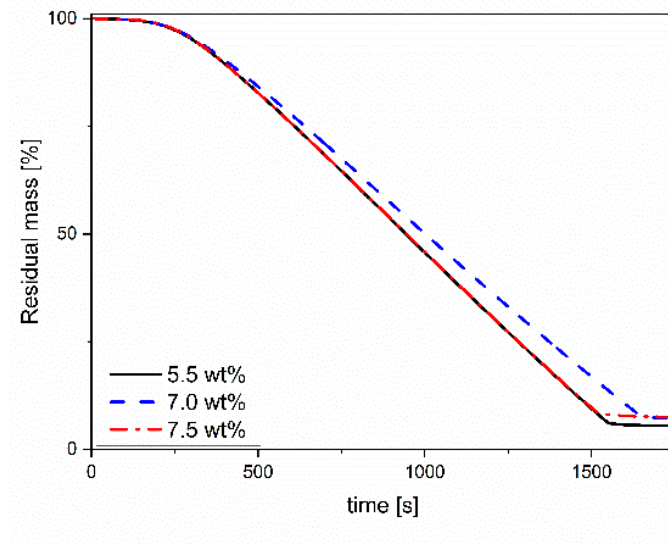
(b)

Figure 3. Effect of the solution concentration on the longest relaxation time for (a) PUL aqueous and hydro-alcoholic solutions prepared using PUL from Batch 1. The concentration is the final PUL concentration. (b) PUL aqueous solutions prepared using PUL from Batch 1 or Batch 2. The concentration reported on the x-axis is expressed as the aqueous solution concentration before dilution with ethanol.

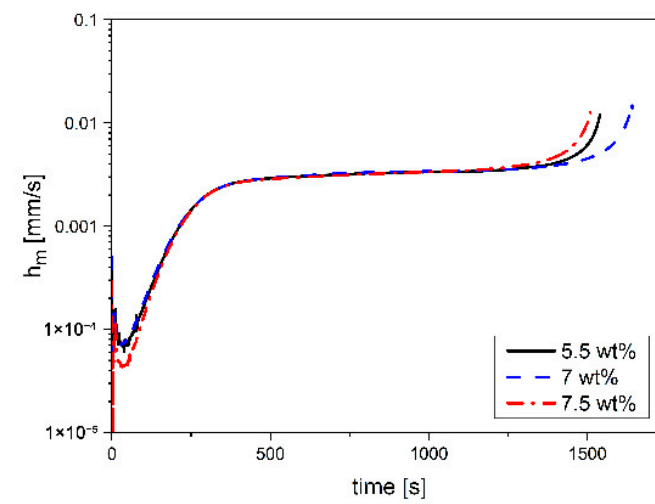
Further, aqueous solutions prepared with PUL from Batch 2 show a longer relaxation time (Figure 3b). Thus, the characterization of extensional behavior allows us to point out subtle differences between the solutions used in this work, which cannot be highlighted by conventional shear rheometry techniques.

3.2. Thermogravimetry Characterization

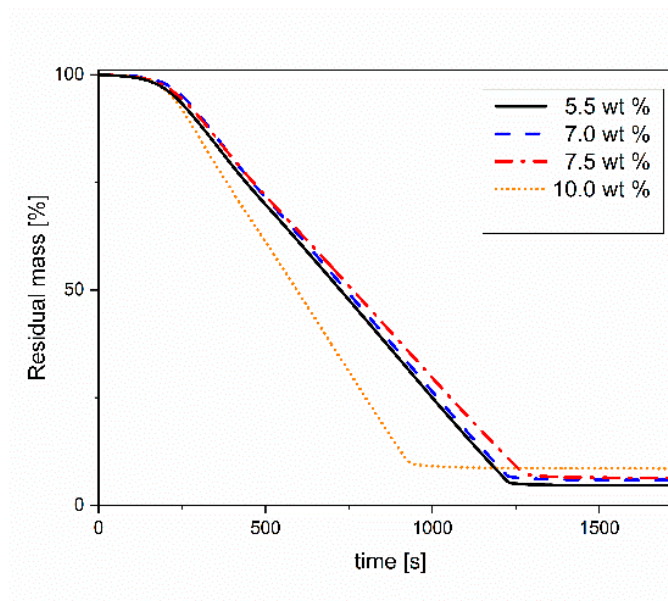
Figure 4 shows the mass loss during thermogravimetric experiments and the change in the mass transfer coefficient, h_m , for aqueous and hydro-alcoholic solutions.



(a)

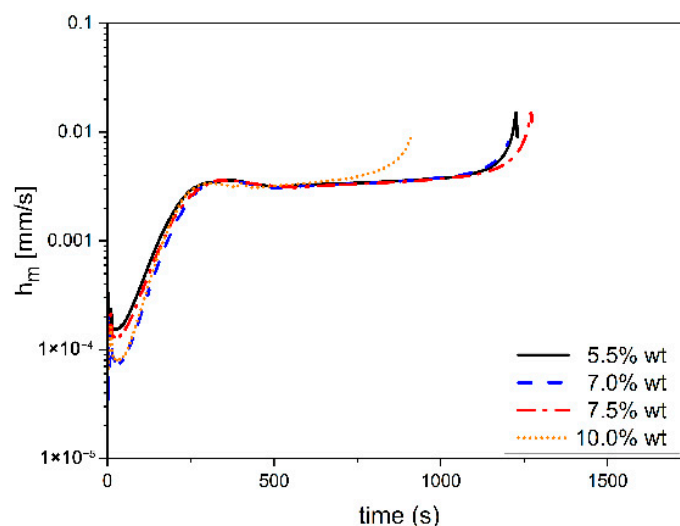


(b)



(c)

Figure 4. Cont.



(d)

Figure 4. TGA experiments on PUL solutions. (a) Solvent mass loss and (b) mass transfer coefficient for aqueous solutions with different concentrations; (c) solvent mass loss; and (d) mass transfer coefficient for hydro-alcoholic solutions with different PUL concentrations. In the case of hydro-alcoholic solutions, the PUL concentration reported is that of the aqueous solution before dilution with EtOH.

The residual masses were consistent with the PUL amount used to prepare the solutions and confirmed that the solvent was completely removed from the sample. Hydro-alcoholic solutions showed a shorter time for complete solvent removal, which could be partly due to a faster release at the beginning of the test, during the increasing temperature ramp. After a sudden increase at the beginning of the experiment, h_m reached a constant plateau, corresponding to the steady state solvent loss.

The mass transfer coefficient, h_m , was not affected by the solution concentration—which may be expected—and is equal to $h_{\text{H}_2\text{O}} = 0.0033 \pm 0.0001$ mm/s and $h_{\text{H}_2\text{O}+\text{EtOH}} = 0.0037 \pm 0.0001$ mm/s. Interestingly, the presence of ethanol had a limited effect on the mass transfer coefficient.

Taking, as a first approximation, $D = 2.21 \times 10^{-7}$ cm²/s, equal to that of PUL in diluted aqueous solutions [22], and the spray drying nozzle diameter as the characteristic length, we estimated a $Pe \approx 100$. This high value suggests that the solvent evaporation dominates over the solute diffusion towards the center of the solution drop. In the thermogravimetric experiments, this is confirmed by the formation of a solid skin, which—in the case of the 10%w/w solution—slowed the evaporation rate at the later stage of the experiment. During the spray drying process, such a high Péclet number is expected to lead to the formation of hollow objects.

3.3. Spray Drying and Particle Observation

Figure 5 shows a selection of the SE microphotographs of the spray-dried powder collected at the end of the process. It can be observed that in some cases (Figure 5, panels b and c), a mixture of fibrils and spheres is present, while in others, only microspheres are obtained. The full set of SE microphotographs are reported in Figures S4 and S5.

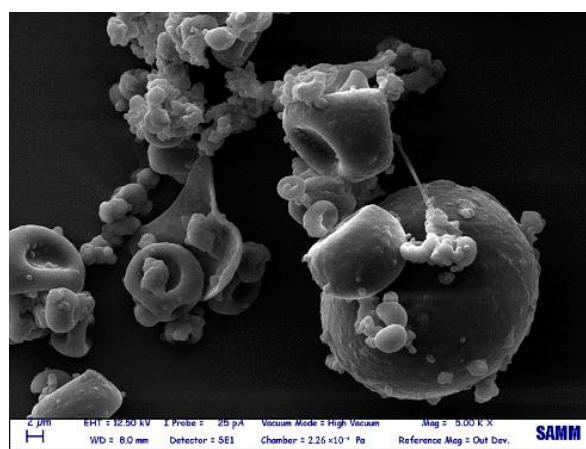
To our knowledge, only the addition of some matrix-forming agents, such as trehalose or leucine, is reported to allow the attainment of spherical morphology [9,11]. In the current case study, no process aids were used, and the result was obtained only by selecting the proper solution concentration. Interestingly, adding ethanol as a co-solvent allowed us to vary the concentration range for microsphere production.

In order to map the concentration range for microsphere production, its whole range was considered, and the results are reported in Table 2. Regarding the aqueous solutions, microspheres were obtained for most of the concentrations considered. Only at a PUL concentration of 5%*w/w* are fibers obtained. The yield was low since most of the material adhered to the drying chamber glass wall before being collected. This is probably due to an incomplete release of water from the PUL particles upon formation within the spray drying.

Table 2. Spray drying of PUL aqueous and hydro-alcoholic solutions. Effect of PUL concentration, batch, and the presence of a co-solvent on the formation of particles (P) or fibers (F).

Nominal Concentration [% <i>w/w</i>]	Batch 1 H ₂ O		Batch 1 H ₂ O + EtOH		Batch 2 H ₂ O + EtOH	
	Longest relax. time λ_c [ms]	Process outcome	Longest relax. time λ_c [ms]	Process outcome	Longest relax. time λ_c [ms]	Process outcome
0.5	==	P	==	P		
1.5	==	P	==	P		
5	==	P + F	==	P		
5.5					0.8 ± 0.1	P
7					1.3 ± 0.2	P + F
7.5	1.0 ± 0.2	P	1.1 ± 0.3	P + F		
10	1.6 ± 0.2	P	2.2 ± 0.3	P + F		
15	7.2 ± 9.8	P	6.5 ± 0.5	P + F		

The high PUL concentration favored the formation of mixed morphologies, while microspheres alone were observed below the mass concentration of 5%*w/w*. Fibrils were formed at two stages: (i) in the spray phase, if the breakup of fluid veins was slowed down by an excessive resistance associated with a high viscosity and elasticity of the viscoelastic fluid and fibrils were stabilized by fast solvent evaporation, or (ii) during the drying phase, if colliding spherical droplets formed an elongated structure. Also, in this case, fast evaporation was needed to stabilize the elongated shape. In the present case, given the configuration of the spray dryer used, the second phenomenon was probably of minor importance because the laminar flow within the drying chamber was expected to limit turbulence and thus droplet collision.

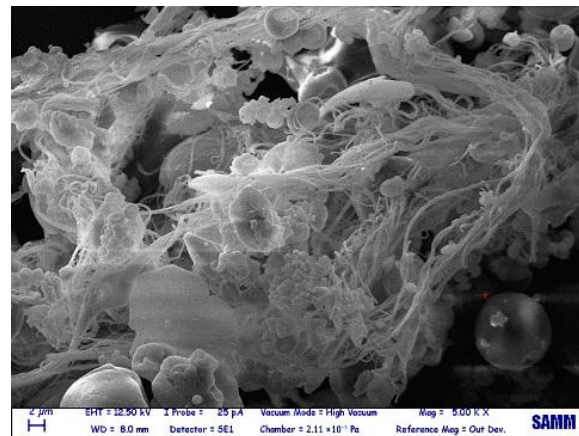


(a)

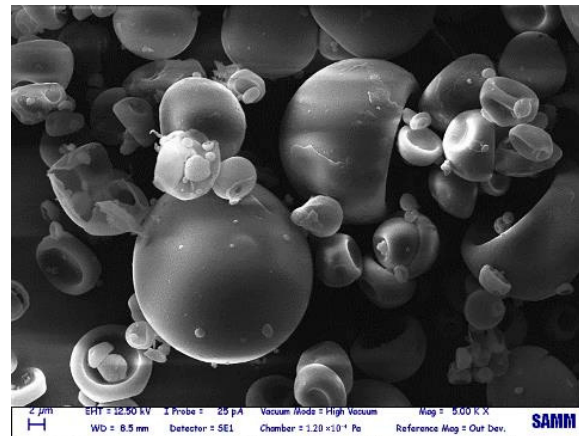
Figure 5. Cont.



(b)



(c)



(d)

Figure 5. SE microphotographs of spray-dried particles obtained from (a,b) aqueous and (c,d) hydro-alcoholic PUL solutions. PUL concentrations before dilution are 7.5%w/w in (a,c) and 5%w/w in (b,d).

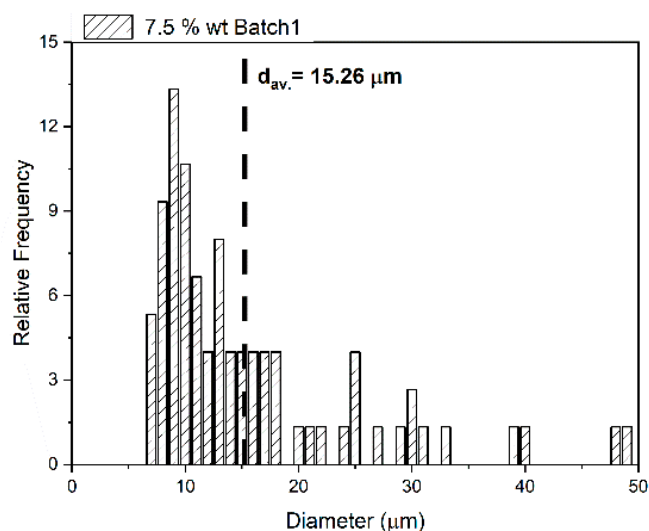
Indeed, the formation and stabilization of fibers were more likely to occur for hydro-alcoholic solutions, which showed a higher elasticity (in terms of relaxation times) at fixed PUL concentrations with respect to aqueous solutions. Further, the mass transfer coefficient for the latter was lower, and as shown by the TGA results (Figure 4), the solvent release was slower at the beginning of the test, while the temperature was still increasing.

To further test the hypothesis that elasticity is the most important factor for fiber formation, spray drying tests were performed on solutions from Batch 2, which showed similar viscosity and higher relaxation times (at the same concentration) with respect to

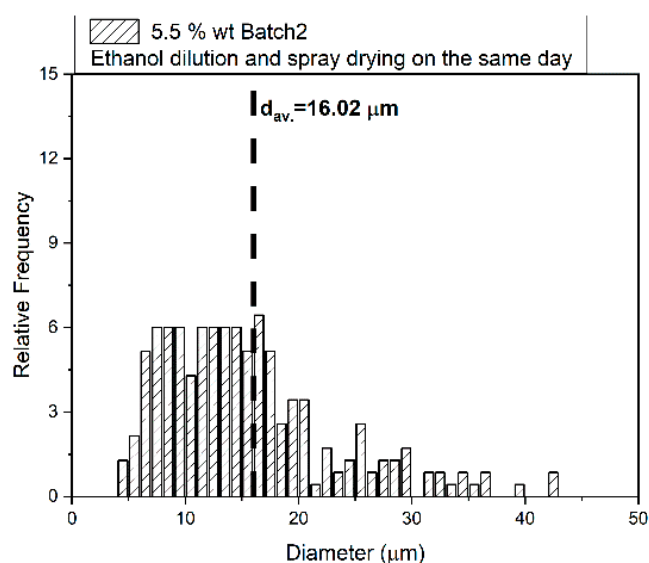
solutions from Batch 1. Table 2 shows that fibrils were already observed at a 7%*w/w* concentration, having a relaxation time higher than that of the 7.5%*w/w* Batch 1 solution, even if the relevant viscosity was lower.

3.4. Particle Size Distribution

As evident in the SE microphotographs, particle size and size distribution could not be determined using conventional methods based on light scattering due to the complexity of particle morphology. Hence, about 150 spherical particles were measured in the microphotographs at 500× magnification in an attempt to have qualitative information on the distribution curve. Despite a relatively small portion of the powder being investigated, the size distribution varied as a function of the PUL concentration, keeping all other parameters constant (Figure 6a,b). Moreover, the storage time of the feed solution (i.e., the time gap between the feed preparation and its processing by spray drying) determined the size of spherical particles (Figure 6c). Since no variations in the rheological properties of feeds were measured over storage time, this feature will be the subject of further investigation.

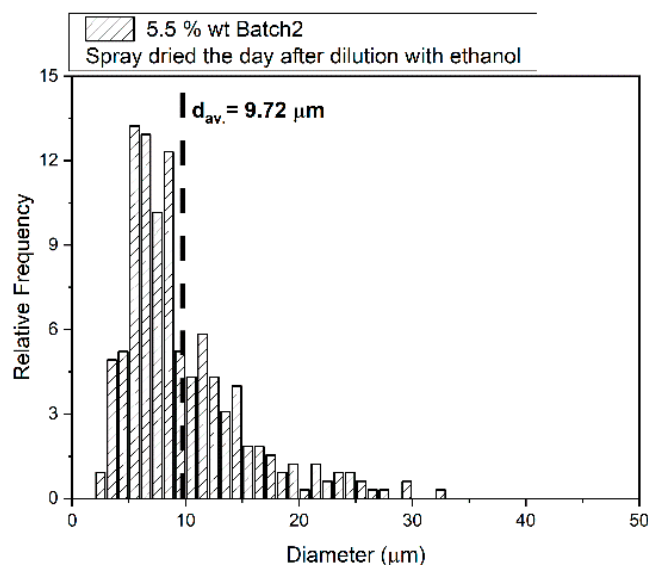


(a)



(b)

Figure 6. Cont.



(c)

Figure 6. Diameter distribution of spheroidal particles obtained from spray drying of (a) Batch 1 PUL 7.5%w/w aqueous solution diluted with ethanol and spray-dried immediately after dilution; (b) Batch 2 PUL 5.5%w/w aqueous solution diluted with ethanol and spray-dried immediately after dilution; (c) Batch 1 PUL 5.5%w/w aqueous solution diluted with ethanol and spray-dried 24 h after dilution.

4. Discussion

The spray-dried powder shape is ruled by the physicochemical characteristics of the feed material and the spray drying process conditions. For most pharmaceutical excipients based on small molecules, the particle shape can be reconducted into spheres, hollow particles, and agglomerates, while for macromolecules, very irregular particles can be obtained. As an example, regenerated keratin [23] and fibroin [24] particles displayed a characteristic raisin-like morphology attributed to the low permeability of solvent upon drying. Regarding cellulose nanofibrils, which are used to reinforce composite materials [25], their shape and size can be tuned by adjusting the spray drying operative conditions [26]. However, the relationship between the operative condition and the final morphology of the powder is not easy to establish. Generally speaking, the atomization increases substantially the surface area of the feed before drying, and the evaporation rate is directly proportional to the droplet surface area. There is not necessarily a direct relationship, but this depends on a combination of factors, including the atomization technology, operating conditions, and the feed compositional and physicochemical properties (e.g., total solids content, rheological behavior, size of dispersed solid, surface tension, and density) [27].

Also, the evaporation of droplets in a spray dryer is a complex phenomenon, involving heat and mass transfer. The drying history can be approximately divided into three stages. Firstly, in “the sensible heating period”, the droplet temperature rapidly increases to an equilibrium temperature, and no appreciable solvent evaporation takes place. Then, the evaporation rate depends on the solvent characteristics and drying conditions and, consequently, the droplet shrinks, causing the diffusion of the solute molecules toward the inner part. As the evaporation progresses, solidification occurs, starting from the surface with the formation of a “skin”. This is the falling rate drying period in which the solvent diffusion through the skin becomes the limiting step of the drying process [28,29]. During this stage, little further shrinkage or skin collapse can occur, depending on the solvent diffusion rate. In this context, P_e , representing the evaporation-to-diffusion rate ratio, allows for predicting whether and when the surface dries to form a skin and, therefore,

the size and density of particles. For $P_e < 1$, evaporation is slower than diffusion, and solute molecules can diffuse toward the center of the droplet, forming small solid particles. Conversely, for high P_e , the fast evaporation results in the accumulation of solids/solutes at the surface and causes early skin formation. This condition leads to large low-density wrinkled and/or hollow particles [28]. It is noteworthy that P_e is not the sole criterion for shell or dense particle formation, and other factors (depending on the equipment design), e.g., feed concentration, surface activity, and solubility level for solutions or solid concentration, may contribute to the particle structure [28].

Given the high P_e for PUL, it is possible to assume that the folded morphology of microparticles can be attributed to the early shell formation upon drying. This result agrees with the radial profile of glass transition temperature for dried particles made of PUL and trehalose since it was predicted and experimentally demonstrated that the glass transition temperature is likely to be higher near the surface due to the higher surface enrichment of PUL as compared to trehalose [9].

From our data, both the feed viscoelasticity and the solvent system composition affected the atomization and solvent evaporation processes. Indeed, the shear viscosity and relaxation time played a major role in determining the morphology—from spheres to fibers without the addition of adjuvants or a chemical modification of the PUL backbone—and the PUL particles' size and morphology. However, size and size distribution are difficult to determine because, in some cases, fibers and particles coexisted and dimples on the surface of bigger particles may nestle smaller ones, causing a high level of dispersity in size.

5. Conclusions

This study shows how the choice of solvent and solute concentration influences the rheological and evaporation behavior of PUL solutions, which strongly affects the spray drying process outcomes. As for the solvent, both water and a mixture of water and ethanol were selected due to the expectation of a different evaporation behavior in the process conditions. Indeed, the addition of the more volatile ethanol has a limited effect on the mass transfer coefficient of the solution, measured at the process temperature by TGA. Further, for both solvents, the solution concentration had no effect on the mass transfer coefficient. In both cases, P_e is significantly higher than unity, indicating that solvent evaporation is faster than solute diffusion, which leads to the formation of hollow particles.

As for the rheological behavior, both aqueous and hydro-alcoholic solutions showed a Newtonian behavior in shear, with the expected increasing viscosity at an increasing PUL concentration. However, when extensional behavior was considered, viscoelastic behavior was evident, and hydro-alcoholic solutions exhibited higher relaxation times than aqueous ones at the same PUL concentration. The investigation of extensional rheology also allowed us to highlight differences in raw PUL batches, which were indistinguishable by shear rheometry. Interestingly, these small differences seem to have a strong effect on the spray-dried powder features. Indeed, if, for aqueous solutions, microsphere formation was observed for almost all samples, for hydro-alcoholic solutions, a transition from microspheres to a mix of fibers and spheres was observed when viscosity and relaxation time increased. This is attributed to the combined effect of resistance to atomization, related to the viscosity and relaxation time increases and the evaporation rate. Given that shear viscosity is independent of the solvent and PUL batch, it might be concluded that the extensional behavior is the main factor responsible for the transition, which is also reflected in the final product particle size distribution. The interplay between evaporation and resistance to atomization needs further investigation, as shown by the unexpected fiber-forming behavior of the 5%w/w aqueous solution and by the modification of size distribution induced by the soaking time after dilution.

Finally, the possibility of tuning the spray-dried product morphology from particles to fibers without any processing aids can pave the way for new applications of PUL, especially in the pharmaceutical sector.

Supplementary Materials: The following supporting information can be downloaded at <https://www.mdpi.com/article/10.3390/polysaccharides6010007/s1>, Figure S1: Viscosity curves for pullulan aqueous (filled points) and hydro-alcoholic (hollow points) at different concentrations. Concentration (%w/w) refers to pullulan concentration in the aqueous solution before dilution with ethanol. The considered shear rates range the solutions display a Newtonian behavior up to a concentration of 10%w/w. Figure S2: Filament evolution during the capillary breakup experiment for an aqueous solution of pullulan (10%w/w). (a) before plate motion $t = 0$; (b) during plate motion, $t = 34$ ms; (c) at $t = 104$ ms; and (d) at $t = 136$ ms, just before breakup. Figure S3: Time evolution of the filament radius (measured at the filament mid-length and normalized with respect to the initial one) versus time for aqueous and hydro-alcoholic pullulan solutions at different concentrations. The arrow indicates the time at which the moving plate reaches its final position; from this point, thinning is driven by the surface tension. The reduction in the thinning rate at times close to breakup indicates the dominance of the elastic response. In this zone, Equation (4) of the manuscript applies. Figure S4: Morphology of powders obtained by the spray drying of pullulan aqueous solutions at different concentrations. Magnification $5000\times$. The nominal concentration is expressed in terms of pullulan % mass in the solution before the dilution with ethanol. Figure S5: Morphology of powders obtained by the spray drying of pullulan hydro-alcoholic solutions at different concentrations. Magnification $5000\times$. The nominal concentration is expressed in terms of pullulan % mass in the solution and is referred to the aqueous solutions before the dilution with ethanol.

Author Contributions: Conceptualization, F.B.V. and F.S.; methodology, F.B.V. and F.S.; software, F.B.V.; validation, F.C.; formal analysis, F.B.V.; investigation, F.B.V. and F.S.; resources, F.B.V. and F.S.; data curation, F.B.V.; writing—original draft preparation, F.B.V.; writing—review and editing, F.C. and F.S.; visualization, F.B.V.; supervision, F.C. All authors have read and agreed to the published version of the manuscript.

Funding: This research received no external funding.

Institutional Review Board Statement: Not applicable.

Data Availability Statement: Data are available upon request from the authors.

Acknowledgments: The authors wish to thank Takanobu Higashiyama from HAYASHIBARA Co., Ltd. for supplying the pullulan material and for the fruitful discussions.

Conflicts of Interest: The authors declare that this study received the pullulan material from Takanobu Higashiyama at the HAYASHIBARA Co., Ltd. The supplier was not involved in the study design, collection, analysis, interpretation of data, the writing of this article, or the decision to submit it for publication.

References

1. Shen, S.; Li, H.; Yang, W. The preliminary evaluation on cholesterol-modified pullulan as a drug nanocarrier. *Drug Deliv.* **2014**, *20*, 501–508. [[CrossRef](#)] [[PubMed](#)]
2. Leathers, T.D. Biotechnological production and applications of pullulan. *Appl. Microb. Biotech.* **2003**, *62*, 468–473. [[CrossRef](#)] [[PubMed](#)]
3. Silva, A.C.Q.; Silvestre, A.J.D.; Vilela, C.; Freire, C.S.R. Natural Polymers-Based Materials: A Contribution to a Greener Future. *Molecules* **2021**, *27*, 94. [[CrossRef](#)] [[PubMed](#)]
4. Farris, S.; Unalan, I.U.; Introzzi, L.; Fuentes-Alventosa, J.M.; Cozzolino, C.A. Pullulan-based films and coatings for food packaging: Present applications, emerging opportunities, and future challenges. *J. Appl. Pol. Sci.* **2014**, *131*, 1–12. [[CrossRef](#)]
5. Musazzi, U.M.; Khalid, G.M.; Selmin, F.; Minghetti, P.; Cilurzo, F. Trends in the production methods of orodispersible films. *Int. J. Pharm.* **2019**, *576*, 118963. [[CrossRef](#)]

6. Ravasi, E.; Melocchi, A.; Arrigoni, A.; Chiappa, A.; Gennari, C.G.M.; Uboldi, M.; Bertarelli, C.; Zema, L.; Briatico Vangosa, F. Electrospinning of pullulan-based orodispersible films containing sildenafil. *Int. J. Pharm.* **2023**, *643*, 123258. [[CrossRef](#)]
7. Fonseca, D.F.S.; Costa, P.C.; Almeida, I.F.; Dias-Pereira, P.; Correia-Sá, I.; Bastos, V.; Oliveira, H.; Duarte-Araújo, M.; Morato, M.; Vilela, C.; et al. Pullulan microneedle patches for the efficient transdermal administration of insulin envisioning diabetes treatment. *Carbohydr. Polym.* **2020**, *241*, 116314. [[CrossRef](#)]
8. Sugandhi, V.V.; Mahajan, H.S. Development of vitamin B12 containing pullulan-bovine serum albumin microparticles designed dry powder inhaler: In-vitro and in-vivo study. *J. Drug Del. Sci. Technol.* **2020**, *70*, 103212. [[CrossRef](#)]
9. Carrigy, N.B.; Ordoubadi, M.; Liu, Y.; Melhem, O.; Barona, D.; Wang, H.; Milburn, L.; Ruzycki, C.A.; Finlay, W.H.; Vehring, R. Amorphous pullulan trehalose microparticle platform for respiratory delivery. *Int. J. Pharm.* **2019**, *563*, 156–168. [[CrossRef](#)]
10. Gomez, M.; McCollum, J.; Wang, H.; Ordoubadi, M.; Jar, C.; Carrigy, N.B.; Barona, D.; Tetreau, I.; Archer, M.; Gerhardt, A.; et al. Development of a formulation platform for a spray-dried, inhalable tuberculosis vaccine candidate. *Int. J. Pharm.* **2021**, *593*, 120121. [[CrossRef](#)]
11. Shruthi, P.A.; Pushpadass, H.A.; Magdaline Eljeeva Emerald, F.; Surendra Nath, B.; Laxmana Naik, N. Formulation and characterization of catechin-loaded proniosomes for food fortification. *J. Sci. Food Agric.* **2021**, *101*, 2439–2448. [[CrossRef](#)] [[PubMed](#)]
12. De Arce Velasquez, A.; Ferreira, L.M.; Stangarlin, M.F.L.; Da Silva, C.D.B.; Rolim, C.M.B.; Cruz, L. Novel Pullulan-Eudragit® S100 blend microparticles for oral delivery of risedronate: Formulation, in vitro evaluation and tableting of blend microparticles. *Mat. Sci. Eng. C* **2014**, *38*, 212–217. [[CrossRef](#)] [[PubMed](#)]
13. Gamble, J.F.; Terada, M.; Holzner, C.; Lavery, L.; Nicholson, S.J.; Timmins, P.; Tobyn, M. Application of X-ray microtomography for the characterisation of hollow polymer-stabilised spray dried amorphous dispersion particles. *Int. J. Pharm.* **2016**, *510*, 1–8. [[CrossRef](#)] [[PubMed](#)]
14. Grosshans, H.; Griesing, M.; Hellwig, T.; Pauer, W.; Moritz, H.U.; Gutheil, E. A new model for the drying of mannitol-water droplets in hot air above the boiling temperature. *Powder Technol.* **2016**, *297*, 259–265. [[CrossRef](#)]
15. Shepard, K.B.; Adam, M.S.; Morgen, M.M.; Mudie, D.M.; Regan, D.T.; Baumann, J.M.; Vodak, D.T. Impact of process parameters on particle morphology and filament formation in spray dried Eudragit L100 polymer. *Powder Technol.* **2020**, *362*, 221–230. [[CrossRef](#)]
16. Colby, R.H. Structure and linear viscoelasticity of flexible polymer solutions: Comparison of polyelectrolyte and neutral polymer solutions. *Rheol. Acta* **2010**, *49*, 425–442. [[CrossRef](#)]
17. Palangetic, L.; Reddy, N.K.; Srinivasan, S.; Cohen, R.E.; McKinley, G.H.; Clasen, C. Dispersity and spinnability: Why highly polydisperse polymer solutions are desirable for electrospinning. *Polymer* **2014**, *55*, 4920–4931. [[CrossRef](#)]
18. Kasaai, M.R. Intrinsic viscosity-molecular weight relationship and hydrodynamic volume for pullulan. *J. Appl. Pol. Sci.* **2006**, *100*, 4325–4332. [[CrossRef](#)]
19. Entov, V.M.; Hinch, E.J. Effect of a spectrum of relaxation times on the capillary thinning of a filament of elastic liquid. *J. Non-Newton. Fluid Mech.* **1997**, *72*, 31–53. [[CrossRef](#)]
20. McKinley, G.H.; Tripathi, A. How to extract the Newtonian viscosity from capillary breakup measurements in a filament rheometer. *J. Rheol.* **2000**, *44*, 653–670. [[CrossRef](#)]
21. James, D.F. Boger Fluids. *Ann. Rev. Fluid Mech.* **2009**, *41*, 129–142. [[CrossRef](#)]
22. Nishinari, K.; Kohyama, K.; Williams, P.A.; Phillips, G.O.; Burchard, W.; Ogino, K. Solution Properties of Pullulan. *Macromolecules* **1991**, *24*, 5590–5593. [[CrossRef](#)]
23. Cilurzo, F.; Selmin, F.; Aluigi, A.; Bellosta, S. Regenerated keratin proteins as potential biomaterial for drug delivery. *Pol. Adv. Technol.* **2013**, *24*, 1025–1028. [[CrossRef](#)]
24. Cilurzo, F.; Gennari, C.G.M.; Selmin, F.; Marotta, L.; Minghetti, P.; Montanari, L. An investigation into silk fibroin conformation in composite materials intended for drug delivery. *Int. J. Pharm.* **2011**, *414*, 218–224. [[CrossRef](#)]
25. Wang, L.; Gramlich, W.; Gardner, D.; Han, Y.; Tajvidi, M. Spray-Dried Cellulose Nanofibril-Reinforced Polypropylene Composites for Extrusion-Based Additive Manufacturing: Nonisothermal Crystallization Kinetics and Thermal Expansion. *J. Comp. Sci.* **2018**, *2*, 7. [[CrossRef](#)]
26. Peng, Y.; Han, Y.; Gardner, D.J. Spray-drying cellulose nanofibrils: Effect of drying process parameters on particle morphology and size distribution. *Wood Fiber Sci.* **2012**, *44*, 448–461.
27. O’Sullivan, J.J.; Norwood, E.A.; O’Mahony, J.A.; Kelly, A.L. Atomisation technologies used in spray drying in the dairy industry: A review. *J. Food Eng.* **2019**, *243*, 57–69. [[CrossRef](#)]

28. Al-Khattawi, A.; Bayly, A.; Phillips, A.; Wilson, D. The design and scale-up of spray dried particle delivery systems. *Expert Opin. Drug Deliv.* **2018**, *15*, 47–63. [[CrossRef](#)]
29. Huang, D. Modeling of Particle Formation during Spray Drying. In Proceedings of the European Drying Conference—EuroDrying'2011, Palma de Mallorca, Spain, 26–28 October 2011.

Disclaimer/Publisher's Note: The statements, opinions and data contained in all publications are solely those of the individual author(s) and contributor(s) and not of MDPI and/or the editor(s). MDPI and/or the editor(s) disclaim responsibility for any injury to people or property resulting from any ideas, methods, instructions or products referred to in the content.